

# All-Optical Matter-Wave Lens using Time-Averaged Potentials

H. Albers,<sup>1</sup> R. Corgier,<sup>1,2,\*</sup> A. Herbst,<sup>1</sup> A. Rajagopalan,<sup>1</sup> C. Schubert,<sup>1,3</sup> C. Vogt,<sup>4</sup> M. Woltmann,<sup>4</sup>  
C. Lämmerzahl,<sup>4</sup> S. Herrmann,<sup>4</sup> E. Charron,<sup>2</sup> W. Ertmer,<sup>1,3</sup> E. M. Rasel,<sup>1</sup> N. Gaaloul,<sup>1</sup> and D. Schlippert<sup>1,†</sup>

<sup>1</sup>*Leibniz Universität Hannover, Institut für Quantenoptik,  
Welfengarten 1, 30167 Hannover, Germany*

<sup>2</sup>*Université Paris-Saclay, CNRS, Institut des Sciences Moléculaires d'Orsay, 91405 Orsay, France*

<sup>3</sup>*Deutsches Zentrum für Luft- und Raumfahrt e.V. (DLR),*

*Institut für Satellitengeodäsie und Inertialsensorik, c/o Leibniz Universität Hannover,  
DLR-SI, Callinstraße 36, 30167, Hannover, Germany*

<sup>4</sup>*ZARM Zentrum für angewandte Raumfahrttechnologie und Mikrogravitation, Universität Bremen,  
Am Fallturm 2, 28359 Bremen, Germany*

(Dated: March 4, 2022)

The stability of matter-wave sensors benefits from interrogating large-particle-number atomic ensembles at high cycle rates. The use of quantum-degenerate gases with their low effective temperatures allows constraining systematic errors towards highest accuracy, but their production by evaporative cooling is costly with regard to both atom number and cycle rate. In this work, we report on the creation of cold matter-waves using a crossed optical dipole trap and shaping it by means of an all-optical matter-wave lens. We demonstrate the trade off between residual kinetic energy and atom number by short-cutting evaporative cooling and estimate the corresponding performance gain in matter-wave sensors. Our method is implemented using time-averaged optical potentials and hence easily applicable in optical dipole trapping setups.

## I. INTRODUCTION

Ever since their first realization, atom interferometers [1–4] have become indispensable tools in fundamental physics [5–17] and inertial sensing [18–30]. The sensitivity of such matter-wave sensors scales with the enclosed space-time area which depends on the momentum transferred by the beam splitters as well as their separation in time. In order to reach long pulse separation times, control systematic shifts, and create ensembles dense enough to detect them after long time-of-flights, the expansion of the atomic clouds needs to be minimized and well controlled. Nevertheless, colder ensembles with lower expansion rates typically need longer preparation times. Therefore, matter-wave sensors require sources with a high flux of large cold atomic ensembles to obtain fast repetition rates. Bose-Einstein condensates (BECs) are investigated to control systematic effects related to residual motion at a level lower than a few parts in  $10^9$  of Earth's gravitational acceleration [20, 31–34]. In addition, due to their narrower velocity distribution [35], BECs offer higher beam splitting efficiencies and thus enhanced contrast [23, 36, 37], especially for large momentum transfer [36, 38–43]. Finally, the inherent atomic collisions present in BECs can enhance matter-wave interferometry by enabling (i) ultra-low expansion rates through collective mode dynamics with a recent demonstration of a 3D expansion energy of  $k_B \cdot 38_{-7}^{+6}$  pK [44], and (ii) ultimately the generation

of mode entanglement through spin-squeezing dynamics to significantly surpass the standard-quantum limit (SQL) [45–48].

Today's fastest BECs sources rely on atom-chip technologies, where near-surface magnetic traps allow for rapid evaporation using radio frequency or microwave transitions. This approach benefits from constant high trapping frequencies during the evaporative cooling process, thus leading to repetition rates on the order of 1 Hz with BECs comprising  $10^5$  atoms [49]. Anyway, since magnetic traps are not suitable in certain situations optical dipole traps (ODTs) become the tool of choice [50]. Examples are trapping of atomic species with low magnetic susceptibility [51, 52], or molecules [53, 54] and composite particles [55, 56], as well as experiments requiring an external magnetic field as a tunable parameter, e.g., when using Feshbach resonances [57]. The intrinsic link between trap depth and trap frequencies in ODTs [58] inhibits runaway evaporation and cold ensembles can be only produced in shallow traps, leading to drastically increased preparation time  $t_P$ . This long standing problem has been recently overcome through the dynamical time-averaged potential (dTAP) technique, where trap depth and trap frequencies can be controlled independently, thus allowing for more efficient and faster evaporation while maintaining high atom numbers [52, 59].

In this work, we use dTAPs for efficient BEC generation and demonstrate an all-optical matter-wave lens capable of further reducing the ensemble's residual kinetic energy. Contrary to pulsed schemes of matter-wave lensing [44, 60–65], we keep the atoms trapped over the entire duration of the matter-wave lens [37], which eases implementation in ground-based sensors. We moreover show that with our technique one can short-cut the evaporation sequence prior to the matter-wave lens, thus increas-

\* LNE-SYRTE, Observatoire de Paris, Université PSL, CNRS, Sorbonne Université 61 avenue de l'Observatoire, 75014 Paris, France

† Email: schlippert@iqo.uni-hannover.de

ing atomic flux by enhancing atom number and reducing cycle time while simultaneously reducing the effective temperature. We show that our method can largely improve the matter-wave sensor’s stability in various application scenarios.

## II. RESULTS

### A. Evaporative cooling

We operate a crossed ODT at a wavelength of 1960 nm loaded from a  $^{87}\text{Rb}$  magneto-optical trap (details in the “Methods” section). Our time-averaged potentials are generated by simultaneous center-position modulation (CPM) of the crossed ODT beams in the horizontal plane. Controlling the amplitude of this modulation and the intensity of the ODT beams enables the dynamic control and decoupling of the trapping frequencies and depth. The waveform of the CPM is chosen in a way that it generates a parabolic potential [52]. Up to  $2 \times 10^7$  rubidium atoms are loaded into the trap with trapping frequencies  $\omega/2\pi \approx \{140; 200; 780\}$  Hz in  $\{x'; y'; z\}$  direction with a trap depth of 170  $\mu\text{K}$ . For this we operate the trap at the maximum achievable laser intensity of 12 W and the CPM at a modulation amplitude of  $h_0 = 140 \mu\text{m}$ . Evaporative cooling is performed by reducing the trap depth exponentially in time while keeping the trapping frequencies at a high level by reducing the amplitude of the CPM. This method allows to generate BECs with up to  $4 \times 10^5$  atoms within 5 s of evaporative cooling. By shortening the time constant of the exponential reduction we generate BECs with  $5 \times 10^4$  ( $2 \times 10^5$ ) particles within 2 s (3 s) of evaporative cooling. At the end of the evaporation sequence the trap frequencies are  $\omega/2\pi \approx \{105; 140; 160\}$  Hz with a depth of about 200 nK. The expansion velocity of the condensate released from the final evaporation trap is  $2 \text{ mm s}^{-1}$ , which corresponds to an effective temperature of 40 nK.

### B. All-optical matter-wave lens

Our matter-wave lens can be applied in any temperature regime explorably in our optical trap. We study its impact on a BEC but also interrupt the evaporation sequence prematurely, thus short-cutting the cycle to use thermal ensembles. To investigate the effect of the lens for different initial expansion temperatures  $T_0$ , we vary the time of evaporative cooling and hold the ensemble in the trap (details in the “Methods” section). We then initiate the matter-wave lens by a rapid decompression [66] in the horizontal directions. This reduces the trapping frequencies from the initial  $\omega_0$  to the frequency of the lensing potential  $\omega_l$  which is on the order of 20% to 60% of  $\omega_0$ . Subsequent oscillations in the trap result in a manipulation in phase space (Fig. 1 a) & b)) for focusing, diffusion, and, importantly collimation of the

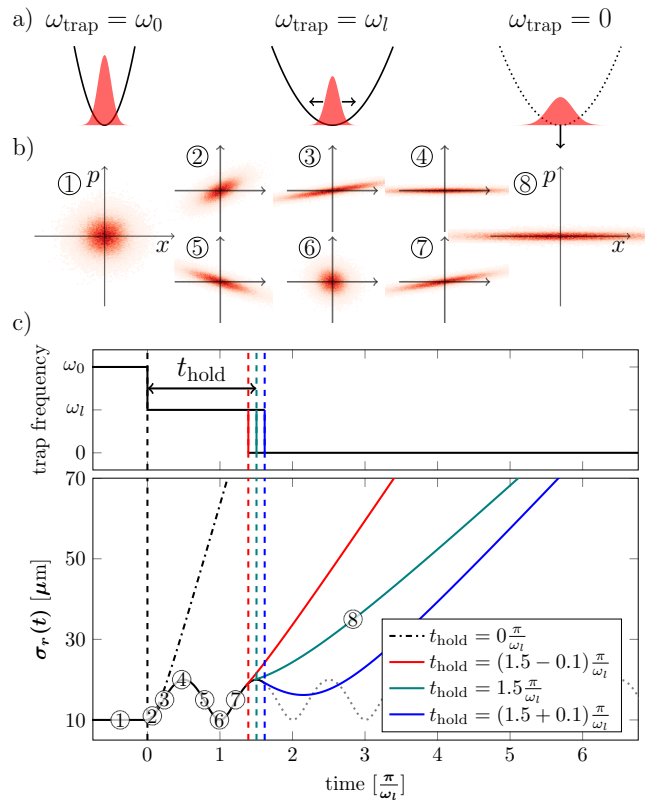


FIG. 1. **Scheme of the matter-wave lens.** The drawing in a) shows the three trap configurations and the distribution of the atomic ensemble during the matter-wave lens. The phase-space diagrams in b) show the atomic distributions at different timings during the matter-wave lens marked with numbers in b) and c). The upper graph in c) shows the behavior of the time dependency of the trapping frequency, while the lower graph shows the simulated evolution of the size of the atomic ensemble. After the holding time in the initial trap the trapping frequency is rapidly decreased at time  $t = 0$  ms. The size of the atomic ensemble starts to oscillate (solid and dotted black line). At time  $t_{\text{hold}} = (n + 0.5) \times \pi/\omega_l$ , with  $n \in \mathbb{N}$ , this oscillation reaches an upper turning point (teal curve). The atomic ensemble is released at its maximum size to minimize its later expansion rate. If the release time ( $t_{\text{hold}}$ ) does not match this condition the expansion rate is not minimized (red and blue curve). The dashed-dotted black curve displays the size of a free falling ensemble without lensing, released at time  $t = 0$  ms.

matter-wave (Fig. 1 c)). Fig. 2 shows exemplary expansion velocities (colored circles) depending on the holding time  $t_{\text{hold}}$ . The colored curves in this graph display the simulated behavior following the scaling approach (details in the “Methods” section) with an error estimation displayed by shaded areas. Only for the final measurement (also shown in the inset in Fig. 2) we create a BEC with a condensed fraction of 92.5% of the total atom number and apply the matter-wave lens to it. With the presented method we observe oscillations of the

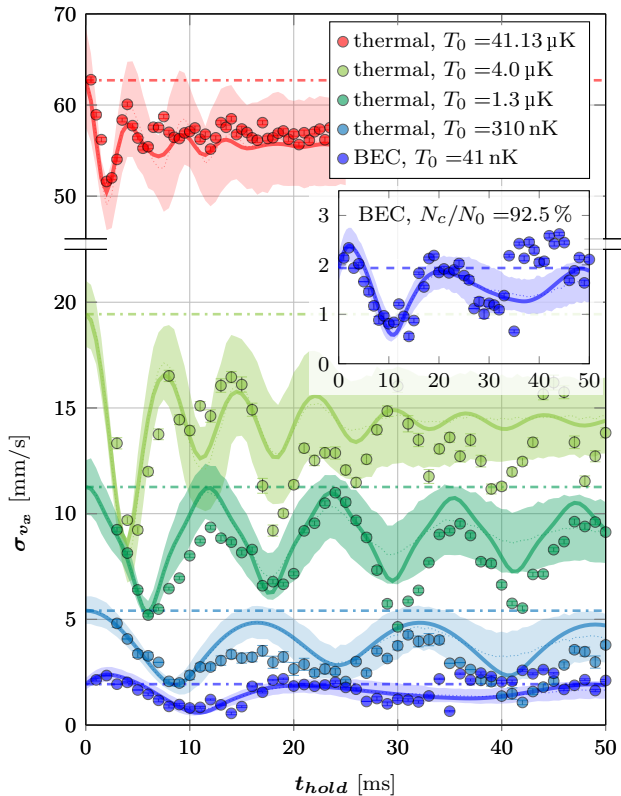


FIG. 2. **Oscillations of expansion velocity.** Expansion velocity after 30 ms of time of flight for different initial temperatures  $T_0$ . The circles show the measurements, the dashed-dotted lines the expansion rate from the initial traps (cf. black dashed-dotted line in Fig. 1). The simulations use the scaling approach and are depicted as lines with a shaded 1-sigma error estimation for the expected trap parameters.

expansion rate in good agreement with the simulations for different temperature regimes accessible by our optical dipole trap. As shown in Fig. 3 for all investigated regimes there exists an optimal holding time for which the final expansion rate is reduced to a value between 20% to 80%.

The change in atom number from the initial to the lens trap (Fig. 3) lies within the error bars and arises mainly due to pointing instabilities of the crossed optical dipole trap beams. The lowest expansion rate is achieved with  $553(49) \mu\text{m s}^{-1}$  with a related effective temperature of  $3.2(0.6) \text{ nK}$  and an atom number of  $4.24(0.02) \times 10^5$ . This is an effective temperature more than one order of magnitude lower than what is achieved by evaporative cooling while maintaining a comparable atom number.

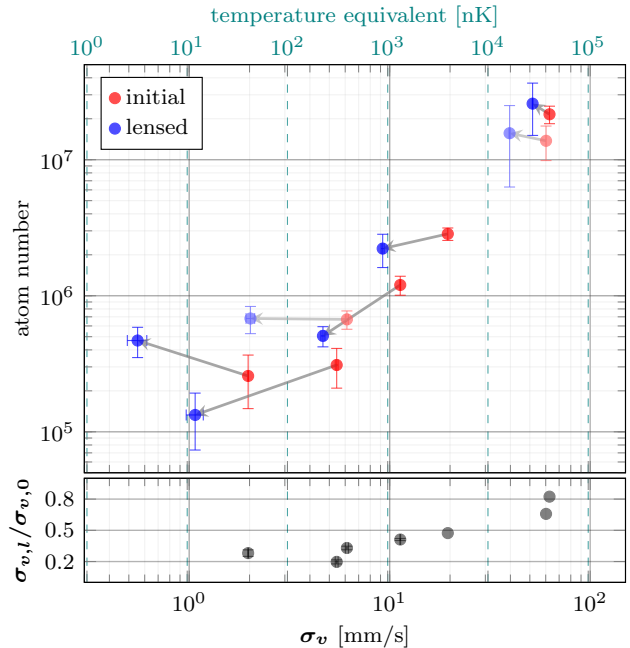


FIG. 3. **Expansion velocity dependent atom number.** Resulting expansion velocity (top graph, blue circles) after the matter-wave lens for different starting temperatures (red circles). The lines connect the corresponding data points. The two grayed out data points associated with the starting expansion velocities  $60 \text{ mm s}^{-1}$  and  $6 \text{ mm s}^{-1}$  are not displayed in Fig. 2 while all the others are included in Fig. 2. The bottom graph shows the ratio of the lensed and the initial ensembles expansion.

### III. DISCUSSION

In this paper we demonstrate a technique to reduce the expansion velocity of an atomic ensemble by rapid decompression and subsequent, release from an ODT at a well-controlled time. The efficiency of the matter-wave lens for higher temperatures is mainly limited by the ratio of the initial and the lensing trap frequency  $\omega_{0,i}/\omega_{l,i}$  (Fig. 3, lower graph), constrained by the maximum CPM amplitude. The evaporative sequence starts with a CPM amplitude of 70% of the maximum value, which was optimized for best loading conditions, and is then decreased. Consequently, the relaxation of the trap is less efficient at the beginning of the evaporative sequence or directly after the loading of the trap. Another constraint is that the trap's confinement in the unpainted vertical direction is required to remain constant since we observe heating effects in case the vertical trap frequency is increased and suffer from atom loss when it is decreased. To compensate for the trap depth reduction during the switch from the initial to the lensing trap we increase the ODT laser's intensity accordingly. An additional modulation in the vertical direction, e.g., by means of a two-dimensional

acousto-optical deflector, as well as an intersection angle of  $90^\circ$  would enable the generation of isotropic dTAP. In such a configuration, the determination of the optimal holding time will benefit from the in-phase oscillations of the atomic ensemble's size [67]. When applying our matter-wave lens in a dual-species experiment, isotropy of the trap will also improve the miscibility of the two ensembles [68]. To illustrate the relevance for atom interferometers, we discuss the impact of our source in different regimes (details in the “Methods” section) at the SQL for an acceleration measurement. In a Mach-Zehnder-like atom interferometer [1, 18], the instability reads

$$\sigma_a(\tau) = \frac{1}{C\sqrt{N}n\hbar k_{\text{eff}}T_1^2} \cdot \sqrt{\frac{t_{\text{cycle}}}{\tau}} \quad (1)$$

after an averaging time  $\tau$ , neglecting the impact of finite pulse durations on the scale factor [69–71]. Eq. (1) scales with the interferometer contrast  $C$ , the atom number per cycle  $N$ , the effective wave number  $n\hbar k_{\text{eff}}$  indicating a momentum transfer during the atom-light interaction corresponding to  $2n$  photons, and the separation time between the interferometer light pulses  $T_1$ . The cycle time of the experiment  $t_{\text{cycle}} = t_P + 2T_1 + t_D$  includes the time for preparing the ensemble  $t_P$ , the interferometer  $2T_1$ , and the detection  $t_D$ . In Eq. (1), the contrast depends on the beam splitting efficiency. This, in turn, is affected by the velocity acceptance and intensity profile of the beam splitting light, both implying inhomogeneous Rabi frequencies, and consequently a reduced mean excitation efficiency [35, 72, 73]. Due to expansion of the atomic ensemble and inhomogeneous excitation, a constrained beam diameter implicitly leads to a dependency of the contrast  $C$  on the pulse separation time  $T_1$ , which we chose as a boundary for our discussion. We keep the effective wave-number fixed and evaluate  $\sigma_a(1\text{ s})$  for different source parameters when varying  $T_1$ . Fig. 4 shows the result for collimated (solid lines) and uncollimated (dotted lines) ensembles in our model (see sec. IV D) and compares them to the instability under use of a molasses-cooled ensemble (dash-dotted line). Up to  $T_1 = 100\text{ ms}$  and  $\sigma_a(1\text{ s}) = 10^{-8}\text{ m s}^{-2}$ , the molasses outperforms evaporatively cooled atoms or BECs due the duration of the evaporation adding to the cycle time and associated losses. In this time regime, the latter can still be beneficial for implementing large momentum transfer beam splitters [36, 38–40, 42, 43] reducing  $\sigma_a(\tau)$  or suppressing systematic errors [20, 31–34, 74] which is not represented in our model and beyond the scope of this paper. According to the curves, exploiting higher  $T_1$  for increased performance requires evaporatively cooled atoms or BECs. This shows the relevance for experiments on large baselines [23, 37, 74–77] or in microgravity [78, 79]. We highlight the extrapolation for the Very Long Baseline Atom Interferometer (VLBAI) [76, 80], targeting a pulse separation time of  $T_1 = 1.2\text{ s}$  [81]. Here, the model describing our source gives the perspective of reaching picokelvin expansion temperatures of matter-wave lensed large atomic en-

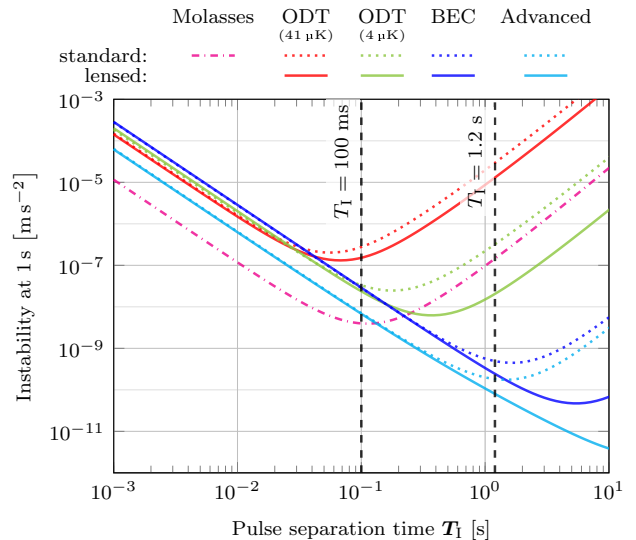


FIG. 4. **Instability comparison.** Behavior of the instability for shot-noise limited atom interferometers after an integration time of  $\tau = 1\text{ s}$  for different sources, see Tab. I, over the pulse separation time  $T_1$ . Except for molasses and the advanced case the colors correspond to the measurements displayed in Fig. 2.

bles.

## IV. METHODS

### A. Experimental Realization

The experimental apparatus is designed to operate simultaneous atom interferometers using rubidium and potassium and is described in detail in references [9, 10, 82]. For the experiments presented in this article only rubidium atoms were loaded from a two dimensional to a three dimensional magneto-optical trap (2D/3D-MOT) situated in our main chamber. After 2 s we turn off the 2D-MOT and compress the atomic ensemble by ramping up the magnetic field gradient as well as the detuning of the cooling laser in the 3D-MOT. Subsequent to compression, the atoms are loaded into the crossed ODT by switching off the magnetic fields and increasing the detuning of the cooling laser to about  $-30\Gamma$ , with  $\Gamma$  being the natural linewidth of the  $D_2$  transition. The setup of our dipole trap is depicted in Fig. 5. The center-position modulation (CPM) is achieved by modulating the frequency driving the AOM (Polytec, ATM-1002FA53.24). The signal for this is generated by a voltage-controlled oscillator (Mini-Circuits, ZOS-150+), driven by a programmable arbitrary-waveform generator (Rigol, DG1022Z). The waveform is chosen to generate a large-volume parabolic potential based on the deriva-

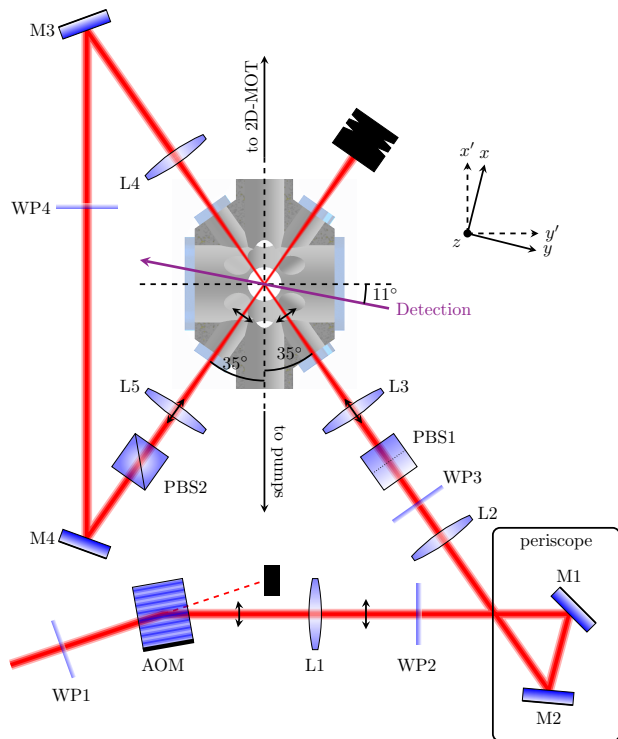


FIG. 5. **Experimental setup.** Optical setup of the ODT and alignment through the vacuum chamber. The AOM is used for CPM and intensity control with WP1 ( $\lambda/2$ ) matching the polarization of the beam for best diffraction. L1 ( $f_1 = 100$  mm) and L2 ( $f_2 = 300$  mm) magnify the beam radius to about 3 mm, 4 mm (vertical, horizontal). L3, L4, and L5 ( $f_{3,4,5} = 150$  mm) focus, re-collimate and re-focus the beam into the center of the chamber. WP3, WP4 ( $\lambda/2$ ), and WP2 ( $\lambda/4$ ) set the polarization for maximum transmission at the orthogonally oriented PBSs (PBS1 and PBS2). The mirrors M1 and M2 form a periscope to guide the beam onto the level of the atoms. M3 and M4 direct the beam a second time through the chamber. The purple arrow indicates the direction of absorption detection along the  $y$ -direction.

tion shown in Ref. [52]. The amplitude of the displacement of the center-position of the dipole trap beam,  $h_0$ , is controlled by regulating the amplitude of the frequency modulation. The CPM yields a maximum displacement of  $h_0 = 200$   $\mu\text{m}$  (300  $\mu\text{m}$ ) at the position of the atoms for the initial (recycled) beam.

## B. Data acquisition and analysis

We apply our matter-wave lens subsequent to loading the dipole trap and evaporative cooling. The duration of the complete evaporative sequence is 5 s for the measurements presented here and was stopped after 0 s, 0.2 s, 1 s, 2 s, 3.5 s, 4.3 s and 5 s. Before the step-wise change of the trap frequency ( $\omega_0 \rightarrow \omega_l$ ) we hold the ensemble in

the trap given by the respective evaporation step configuration for 50 ms. The oscillations of the expansion rate after the matter-wave lens are observed by measuring the ensemble's radius by means of absorption imaging with iterating  $t_{\text{hold}}$  and different times after release from the trap. For each holding time the expansion velocity is extracted by fitting a ballistic expansion. This measurement is performed for different starting temperatures in the thermal regime as well as a BEC. The simulations shown in figure 2 use the scaling approach as described in Sec. IV C. Here, the trapping frequencies of the lens potential in  $x$ - and  $y$ -direction have been extracted by fitting two damped oscillations to the measured data. The starting expansion velocity was set by choosing a reasonable initial radius of the ensemble (Table I). The other parameters arise from the measurements or simulations of the trapping potentials. The shaded areas in figure 2 depict an error estimation of the expansion velocity oscillations obtained from performing the simulation by randomly choosing input parameters from within the error bars for 1000 simulation runs and calculating the mean value as well as the standard deviation for each  $t_{\text{hold}}$ .

## C. Scaling Approach

The dynamics of an ideal gas can be described using the scaling approach [83, 84]. The size of the ensemble scales with the time dependent dimensionless factor  $b_i(t)$ .

$$\ddot{b}_i(t) + \omega_i^2(t)b_i(t) - \omega_{0,i}^2 \frac{\theta_i(t)}{b_i(t)} + \omega_{0,i}^2 \xi \left( \frac{\theta_i(t)}{b_i(t)} - \frac{1}{b_i(t) \prod_j b_j(t)} \right) = 0 \quad (2)$$

$$\dot{\theta}_i(t) + 2 \frac{\dot{b}_i(t)}{b_i(t)} \theta_i(t) + \frac{1}{\tau} \left( \theta_i(t) - \frac{1}{3} \sum_j \theta_j(t) \right) = 0 \quad (3)$$

where  $\theta_i$  acts as an effective temperature in the directions  $i \in x, y, z$ . Here  $\omega_{0,i}$  denotes the initial angular trap frequency and  $\omega_i(t)$  denotes the time-dependent angular trap frequency defined such as:  $0 < t < t_{\text{hold}}$   $\omega_i(t) = \omega_{l,i}$ , with  $\omega_{l,i}$  being the lensing potential, and  $\omega_i(t) = 0$  afterward (see Fig.1). This system of six coupled differential equations contains the mean field interaction, given by the factor:

$$\xi = \frac{E_{mf}}{E_{mf} + k_B T} \quad (4)$$

with

$$E_{mf} = \frac{4\pi\hbar^2 a_s n_0}{m} \quad (5)$$

were  $a_s$  is the s-wave scattering length,  $n_0$  the peak density and  $m$  the mass of a single particle. Collision effects are also taken into account through

$$\tau = \tau_0 \times \left( \prod_j b_j \right) \times \left( \frac{1}{3} \sum_k \theta_k \right) \quad (6)$$

with the relaxation time

$$\tau_0 = \frac{5}{4\gamma} \quad (7)$$

and [84]

$$\gamma = \frac{2}{\sqrt{2\pi}} n_0 \sigma_{coll} \sqrt{\frac{k_B T}{m}} \quad (8)$$

For the special case of a BEC the mean field energy is large compared to the thermal ensemble's energy ( $\xi \approx 1$ ) and the time scale on which collisions appear goes to zero ( $\tau \approx 0$ ). Eq. (2) will turn into the form known from Ref. [85].

With this set of equations the time evolution of the ensemble's size ( $\sigma_{r_i}$ ) and velocity distribution ( $\sigma_{v_i}$ ) is determined during the entire sequence of our matter-wave lensing sequence by

$$\sigma_{r_i}(t) = \sigma_{r_i}(0) \times b_i(t) \quad (9)$$

and

$$\sigma_{v_i}(t) = \frac{d\sigma_{r_i}(t)}{dt} \quad (10)$$

The scaling parameter  $b_i$  can be applied either on the radius of a gaussian shaped thermal ensemble or the Thomas-Fermi radius of a BEC. For a long enough freely evolving ensemble the expansion rate is given by the velocity distribution which can be transformed into an effective temperature using:

$$\sigma_{v_i}^2 = \frac{k_B T_i}{m} \quad (11)$$

along each direction. For the case of a thermal ensemble the time evolution of the size and velocity spread in 1D is depicted in Fig. 1 for three different holding times ( $t_{\text{hold}}$ ) to highlight the importance of a well chosen timing for the lens.

#### D. Estimation of instability in matter-wave sensors

The instability of a matter-wave sensor operating at the SQL can be estimated using Eq. (1). Here we assumed Raman beam splitters ( $n = 1$ ) with a  $1/e^2$ -radius of 1.2 cm and a pulse duration of  $t_\pi = 15 \mu\text{s}$ . The contrast ( $C$ ) is taken into account as the product of the excitation probabilities of the atom-light interactions during the Mach-Zehnder type interferometer following [72]. Table I shows the source parameters used for the estimation of the instability. Except for the molasses and the advanced scenario this table contains the parameters measured in our experiment. For the molasses we choose parameters that reasonably fit our experiment combined with a velocity selective Raman pulse of  $30 \mu\text{s}$  [73]. In the advanced scenario we assume a BEC with  $1 \times 10^6$  atoms

TABLE I. **Source parameters for instability estimation.** The values for the ensemble radius ( $\sigma_r$ ) and expansion velocity ( $\sigma_v$ ) are given for the horizontal (h) and vertical (v) direction, which corresponds to the transverse and longitudinal direction of the beam splitter respectively.

	$\sigma_r$ (h/v) [ $\mu\text{m}$ ]	$\sigma_v$ (h/v) [ $\text{mm s}^{-1}$ ]	$N$	$t_P$ s
Molasses	750/750	30.9/30.9	$4 \times 10^8$	2
ODT (41 $\mu\text{K}$ )	65/6.2	62.7/44.5	$2.3 \times 10^7$	2.7
ODT (41 $\mu\text{K}$ ) lensed	86/7.6	51.5/40.8	$2.2 \times 10^7$	2.7
ODT (4 $\mu\text{K}$ )	15.2/12.2	19.6/12	$2.7 \times 10^6$	4.7
ODT (4 $\mu\text{K}$ ) lensed	49/12.2	9.2/12.9	$2.6 \times 10^6$	4.7
BEC	3.8/3.3	2/2	$4.3 \times 10^5$	8.2
BEC lensed	16.9/3.3	0.55/2.2	$4.2 \times 10^5$	8.2
Advanced	5/5	2/2	$1 \times 10^6$	1
Advanced lensed	46.1/46.1	0.14/0.14	$1 \times 10^6$	1

after a preparation time  $t_P = 1 \text{ s}$  with a starting expansion velocity of  $2 \text{ mm s}^{-1}$ , as anticipated for the VLBAI setup [76, 80]. After the lens the resulting expansion velocity is  $0.135 \text{ mm s}^{-1}$  corresponding to an equivalent 3D temperature of 200 pK.

#### DATA AVAILABILITY

The data used in this manuscript are available from the corresponding author upon reasonable request.

[1] M. Kasevich and S. Chu, Atomic interferometry using stimulated raman transitions, *Physical Review Letters* **67**, 181 (1991).  
 [2] M. Kasevich and S. Chu, Measurement of the gravitational acceleration of an atom with a light-pulse atom interferometer, *Appl. Phys. B* **54**, 321 (1992).

[3] F. Riehle, T. Kisters, A. Witte, J. Helmcke, and C. J. Bordé, Optical ramsey spectroscopy in a rotating frame: Sagnac effect in a matter-wave interferometer, *Phys. Rev. Lett.* **67**, 177 (1991).  
 [4] A. D. Cronin, J. Schmiedmayer, and D. E. Pritchard, Optics and interferometry with atoms and molecules, *Reviews of Modern Physics* **81**, 1051 (2009).

- [5] G. W. Biedermann, X. Wu, L. Deslauriers, S. Roy, C. Mahadeswaraswamy, and M. A. Kasevich, Testing gravity with cold-atom interferometers, *Physical Review A* **91**, 10.1103/physreva.91.033629 (2015).
- [6] R. Bouchendira, P. Cladé, S. Guellati-Khélifa, F. Nez, and F. Biraben, New determination of the fine structure constant and test of the quantum electrodynamics, *Physical Review Letters* **106**, 10.1103/physrevlett.106.080801 (2011).
- [7] R. H. Parker, C. Yu, W. Zhong, B. Estey, and H. Müller, Measurement of the fine-structure constant as a test of the standard model, *Science* **360**, 191 (2018).
- [8] T. Damour, Testing the equivalence principle: why and how?, *Class. Quantum Grav.* **13**, A33 (1996).
- [9] D. Schlippert, J. Hartwig, H. Albers, L. Richardson, C. Schubert, A. Roura, W. Schleich, W. Ertmer, and E. Rasel, Quantum test of the universality of free fall, *Phys. Rev. Lett.* **112**, 203002 (2014).
- [10] H. Albers, A. Herbst, L. L. Richardson, H. Heine, D. Nath, J. Hartwig, C. Schubert, C. Vogt, M. Woltmann, C. Lämmerzahl, S. Herrmann, W. Ertmer, E. M. Rasel, and D. Schlippert, Quantum test of the universality of free fall using rubidium and potassium, *The European Physical Journal D* **74**, 10.1140/epjd/e2020-10132-6 (2020).
- [11] S. Fray, C. A. Diez, T. Haensch, and M. Weitz, Atomic interferometer with amplitude gratings of light and its applications to atom based tests of the equivalence principle, *Phys. Rev. Lett.* **93**, 240404 (2004).
- [12] A. Bonnin, N. Zahzam, Y. Bidel, and A. Bresson, Simultaneous dual-species matter-wave accelerometer, *Phys. Rev. A* **88**, 043615 (2013).
- [13] C. Kuhn, G. McDonald, K. Hardman, S. Bennetts, P. Everitt, P. Altin, J. Debs, J. Close, and N. Robins, A bose-condensed, simultaneous dual-species mach-zehnder atom interferometer, *New J. Phys.* **16**, 073035 (2014).
- [14] M. Tarallo, T. Mazzoni, N. Poli, D. Sutyryn, X. Zhang, and G. Tino, Test of einstein equivalence principle for 0-spin and half-integer-spin atoms: Search for spin-gravity coupling effects, *Phys. Rev. Lett.* **113**, 023005 (2014).
- [15] L. Zhou, S. Long, B. Tang, X. Chen, F. Gao, W. Peng, W. Duan, J. Zhong, Z. Xiong, J. Wang, Y. Zhang, and M. Zhan, Test of equivalence principle at  $10^{-8}$  level by a dual-species double-diffraction raman atom interferometer, *Physical Review Letters* **115**, 10.1103/physrevlett.115.013004 (2015).
- [16] P. Asenbaum, C. Overstreet, M. Kim, J. Curti, and M. A. Kasevich, Atom-interferometric test of the equivalence principle at the 10-12 level, *Physical Review Letters* **125**, 191101 (2020).
- [17] G. M. Tino, Testing gravity with cold atom interferometry: results and prospects, *Quantum Science and Technology* **6**, 024014 (2021).
- [18] A. Peters, K. Y. Chung, and S. Chu, Measurement of gravitational acceleration by dropping atoms, *Nature* **400**, 849 (1999).
- [19] A. Peters, K.-Y. Chung, and S. Chu, High-precision gravity measurements using atom interferometry, *Metrologia* **38**, 25 (2001).
- [20] A. Louchet-Chauvet, T. Farah, Q. Bodart, A. Clairon, A. Landragin, S. Merlet, and F. P. D. Santos, The influence of transverse motion within an atomic gravimeter, *New Journal of Physics* **13**, 065025 (2011).
- [21] C. Freier, M. Hauth, V. Schkolnik, B. Leykauf, M. Schilling, H. Wziontek, H.-G. Scherneck, J. Müller, and A. Peters, Mobile quantum gravity sensor with unprecedented stability, *J. Phys. Conf. Ser.* **723**, 012050 (2016).
- [22] B. Barrett, L. Antoni-Micollier, L. Chichet, B. Battelier, T. Lévêque, A. Landragin, and P. Bouyer, Dual matter-wave inertial sensors in weightlessness, *Nat. Commun.* **7**, 13786 (2016) 10.1038/ncomms13786 (2016).
- [23] K. Hardman *et al.*, Simultaneous precision gravimetry and magnetic gradiometry with a bose-einstein condensate: A high precision, quantum sensor, *Phys. Rev. Lett.* **117**, 138501 (2016).
- [24] M. Gersemann, M. Gebbe, S. Abend, C. Schubert, and E. M. Rasel, Differential interferometry using a Bose-Einstein condensate, *Eur. Phys. J. D* **74**, 203 (2020).
- [25] D. Savoie, M. Altorio, B. Fang, L. A. Sidorenkov, R. Geiger, and A. Landragin, Interleaved atom interferometry for high-sensitivity inertial measurements, *Science Advances* **4**, eaau7948 (2018).
- [26] P. Berg, S. Abend, G. Tackmann, C. Schubert, E. Giese, W. Schleich, F. Narducci, W. Ertmer, and E. Rasel, Composite-light-pulse technique for high-precision atom interferometry, *Physical Review Letters* **114**, 10.1103/physrevlett.114.063002 (2015).
- [27] J. Stockton, K. Takase, and M. Kasevich, Absolute geodetic rotation measurement using atom interferometry, *Phys. Rev. Lett.* **107**, 133001 (2011).
- [28] A. Gauguier, B. Canuel, T. Lévêque, W. Chaïbi, and A. Landragin, Characterization and limits of a cold-atom sagnac interferometer, *Physical Review A* **80**, 10.1103/physreva.80.063604 (2009).
- [29] B. Canuel, F. Leduc, D. Holleville, A. Gauguier, J. Fils, A. Virdis, A. Clairon, N. Dimarcq, C. Bordé, A. Landragin, and P. Bouyer, Six-axis inertial sensor using cold-atom interferometry, *Phys. Rev. Lett.* **97**, 010402 (2006).
- [30] R. Geiger, A. Landragin, S. Merlet, and F. P. D. Santos, High-accuracy inertial measurements with cold-atom sensors, *AVS Quantum Science* **2**, 024702 (2020).
- [31] T. Hensel, S. Loriani, C. Schubert, F. Fitzek, S. Abend, H. Ahlers, J. N. Siemß, K. Hammerer, E. M. Rasel, and N. Gaaloul, Inertial sensing with quantum gases: a comparative performance study of condensed versus thermal sources for atom interferometry, *The European Physical Journal D* **75**, 10.1140/epjd/s10053-021-00069-9 (2021).
- [32] N. Heine, M. Matthias, J. andl Sahelgozin, W. Herr, S. Abend, L. Timmen, J. Müller, and E. M. Rasel, A transportable quantum gravimeter employing delta-kick collimated bose-einstein condensates, *Eur. Phys. J. D* **74**, 174 (2020).
- [33] R. Karcher, A. Imanaliev, S. Merlet, and F. Pereira Dos Santos, Improving the accuracy of atom interferometers with ultracold sources, *New J. Phys.* **20**, 113041 (2018).
- [34] V. Schkolnik, B. Leykauf, M. Hauth, C. Freier, and A. Peters, The effect of wavefront aberrations in atom interferometry, *Appl. Phys. B* **120**, 311 (2015).
- [35] S. S. Zsigeti, J. E. Debs, J. J. Hope, N. P. Robins, and J. D. Close, Why momentum width matters for atom interferometry with bragg pulses, *New Journal of Physics* **14**, 023009 (2012).
- [36] S. Abend, M. Gebbe, M. Gersemann, H. Ahlers, H. Müntinga, E. Giese, N. Gaaloul, C. Schubert, C. Lämmerzahl, W. Ertmer, W. P. Schleich, and E. M. Rasel, Atom-chip fountain gravimeter, *Phys. Rev. Lett.*

- 117**, 203003 (2016).
- [37] S. M. Dickerson, J. M. Hogan, A. Sugarbaker, D. M. S. Johnson, and M. A. Kasevich, Multiaxis inertial sensing with long-time point source atom interferometry, *Physical Review Letters* **111**, 10.1103/physrevlett.111.083001 (2013).
- [38] M. Gebbe, J.-N. Siemß, M. Gersemann, H. Müntinga, S. Herrmann, C. Lämmerzahl, H. Ahlers, N. Gaaloul, C. Schubert, K. Hammerer, S. Abend, and E. M. Rasel, Twin-lattice atom interferometry, *Nature Communications* **12**, 10.1038/s41467-021-22823-8 (2021).
- [39] G. D. McDonald, C. C. N. Kuhn, S. Bennetts, J. E. Debs, K. S. Hardman, M. Johnsson, J. D. Close, and N. P. Robins,  $80\hbar k$  momentum separation with bloch oscillations in an optically guided atom interferometer, *Physical Review A* **88**, 10.1103/physreva.88.053620 (2013).
- [40] S.-w. Chiow, T. Kovachy, H.-C. Chien, and M. Kasevich,  $102\hbar k$  Large Area Atom Interferometers, *Phys. Rev. Lett.* **107**, 130403 (2011).
- [41] J. Debs, P. Altin, T. Barter, D. Döring, G. Dennis, G. McDonald, R. Anderson, J. Close, and N. Robins, Cold-atom gravimetry with a bose-einstein condensate, *Phys. Rev. A* **84**, 033610 (2011).
- [42] S.-w. Chiow, S. Herrmann, S. Chu, and H. Müller, Noise-immune conjugate large-area atom interferometers, *Phys. Rev. Lett.* **103**, 050402 (2009).
- [43] P. Cladé, S. Guellati-Khélifa, F. Nez, and F. Biraben, Large momentum beam splitter using bloch oscillations, *Phys. Rev. Lett.* **102**, 240402 (2009).
- [44] C. Deppner, W. Herr, M. Cornelius, P. Stromberger, T. Sterneke, C. Grzeschik, A. Grote, J. Rudolph, S. Herrmann, M. Krutzik, A. Wenzlawski, R. Corgier, E. Charron, D. Guéry-Odelin, N. Gaaloul, C. Lämmerzahl, A. Peters, P. Windpassinger, and E. M. Rasel, Collective-mode enhanced matter-wave optics, *Phys. Rev. Lett.* **127**, 100401 (2021).
- [45] I. Kruse, K. Lange, J. Peise, B. Lücke, L. Pezzè, J. Arlt, W. Ertmer, C. Lisdat, L. Santos, A. Smerzi, and C. Klempt, Improvement of an atomic clock using squeezed vacuum, *Phys. Rev. Lett.* **117**, 143004 (2016).
- [46] S. S. Szigeti, S. P. Nolan, J. D. Close, and S. A. Haine, High-precision quantum-enhanced gravimetry with a bose-einstein condensate, *Physical Review Letters* **125**, 100402 (2020).
- [47] F. Anders, A. Idel, P. Feldmann, D. Bondarenko, S. Loriani, K. Lange, J. Peise, M. Gersemann, B. Meyer, S. Abend, N. Gaaloul, C. Schubert, D. Schlippert, L. Santos, E. Rasel, and C. Klempt, Momentum entanglement for atom interferometry, *ArXiv* (2020), arXiv:2010.15796 [quant-ph].
- [48] R. Corgier, N. Gaaloul, A. Smerzi, and L. Pezzè, Delta-kick squeezing, *ArXiv* (2021), arXiv:2103.10896 [quant-ph].
- [49] J. Rudolph *et al.*, A high-flux bec source for mobile atom interferometers, *New J. Phys.* **17**, 065001 (2015).
- [50] S. Chu, J. E. Bjorkholm, A. Ashkin, and A. Cable, Experimental observation of optically trapped atoms, *Physical Review Letters* **57**, 314 (1986).
- [51] S. Stellmer, R. Grimm, and F. Schreck, Production of quantum-degenerate strontium gases, *Phys. Rev. A* **87**, 013611 (2013).
- [52] R. Roy, A. Green, R. Bowler, and S. Gupta, Rapid cooling to quantum degeneracy in dynamically shaped atom traps, *Phys. Rev. A* **93**, 043403 (2016).
- [53] L. Anderegg, B. L. Augenbraun, Y. Bao, S. Burchesky, L. W. Cheuk, W. Ketterle, and J. M. Doyle, Laser cooling of optically trapped molecules, *Nature Physics* **14**, 890 (2018).
- [54] L. D. Carr, D. DeMille, R. V. Krems, and J. Ye, Cold and ultracold molecules: science, technology and applications, *New Journal of Physics* **11**, 055049 (2009).
- [55] R. Grimm, M. Weidemüller, and Y. B. Ovchinnikov, Optical dipole traps for neutral atoms, in *Advances In Atomic, Molecular, and Optical Physics*, Vol. 42 (Elsevier, 2000) pp. 95–170.
- [56] I. A. Martínez, A. Petrosyan, D. Guéry-Odelin, E. Trizac, and S. Ciliberto, Engineered swift equilibration of a brownian particle, *Nature Physics* **12**, 843 (2016).
- [57] G. Salomon, L. Fouché, S. Lepoutre, A. Aspect, and T. Bourdel, All-optical cooling of  $K39t$  to bose-einstein condensation, *Physical Review A* **90**, 10.1103/physreva.90.033405 (2014).
- [58] K. M. O’Hara, M. E. Gehm, S. R. Granade, and J. E. Thomas, Scaling laws for evaporative cooling in time-dependent optical traps, *Physical Review A* **64**, 051403 (2001).
- [59] G. Condon, M. Rabault, B. Barrett, L. Chichet, R. Arguel, H. Eneriz-Imaz, D. Naik, A. Bertoldi, B. Battelier, P. Bouyer, and A. Landragin, All-optical bose-einstein condensates in microgravity, *Physical Review Letters* **123**, 10.1103/physrevlett.123.240402 (2019).
- [60] H. Ammann and N. Christensen, Delta kick cooling: A new method for cooling atoms, *Phys. Rev. Lett.* **78**, 2088 (1997).
- [61] M. Morinaga, I. Bouchoule, J.-C. Karam, and C. Salomon, Manipulation of motional quantum states of neutral atoms, *Physical Review Letters* **83**, 4037 (1999).
- [62] S. H. Myrskog, J. K. Fox, H. S. Moon, J. B. Kim, and A. M. Steinberg, Modified “ $\delta$ -kick cooling” using magnetic field gradients, *Physical Review A* **61**, 10.1103/physreva.61.053412 (2000).
- [63] T. Luan, Y. Li, X. Zhang, and X. Chen, Realization of two-stage crossed beam cooling and the comparison with delta-kick cooling in experiment, *Review of Scientific Instruments* **89**, 123110 (2018).
- [64] S. Kanthak, M. Gebbe, M. Gersemann, S. Abend, E. M. Rasel, and M. Krutzik, Time-domain optics for atomic quantum matter, *New Journal of Physics* **23**, 093002 (2021).
- [65] D. Gochnauer, T. Rahman, A. Wirth-Singh, and S. Gupta, Interferometry in an atomic fountain with ytterbium bose-einstein condensates, *Atoms* **9**, 10.3390/atoms9030058 (2021).
- [66] S. Chu, J. E. Bjorkholm, A. Ashkin, J. P. Gordon, and L. W. Hollberg, Proposal for optically cooling atoms to temperatures of the order of  $10^{-6}$  k, *Optics Letters* **11**, 73 (1986).
- [67] R.-Z. Li, T.-Y. Gao, D.-F. Zhang, S.-G. Peng, L.-R. Kong, X. Shen, and K.-J. Jiang, Expansion dynamics of a spherical bose-einstein condensate, *Chinese Physics B* **28**, 106701 (2019).
- [68] R. Corgier, S. Loriani, H. Ahlers, K. Posso-Trujillo, C. Schubert, E. M. Rasel, E. Charron, and N. Gaaloul, Interacting quantum mixtures for precision atom interferometry, *New Journal of Physics* **22**, 123008 (2020).
- [69] A. Bertoldi, F. Minardi, and M. Prevedelli, Phase shift in atom interferometers: Corrections for nonquadratic potentials and finite-duration laser pulses, *Phys. Rev. A*



- 99, 033619 (2019).
- [70] C. Antoine, Rotating matter-wave beam splitters and consequences for atom gyroscopes, *Phys. Rev. A* **76**, 033609 (2007).
- [71] P. Cheinet, B. Canuel, F. Pereira Dos Santos, A. Gauget, F. Yver-Leduc, and A. Landragin, Measurement of the sensitivity function in a time-domain atomic interferometer, *Instrumentation and Measurement, IEEE Transactions on*, *IEEE Trans. Instrum. Meas.* **57**, 1141 (2008).
- [72] S. Loriani, D. Schlippert, C. Schubert, S. Abend, H. Ahlers, W. Ertmer, J. Rudolph, J. M. Hogan, M. A. Kasevich, E. M. Rasel, and N. Gaaloul, Atomic source selection in space-borne gravitational wave detection, *New Journal of Physics* **21**, 063030 (2019).
- [73] M. Kasevich, D. Weiss, E. Riis, K. Moler, S. Kasapi, and S. Chu, Atomic velocity selection using stimulated raman transitions, *Phys. Rev. Lett.* **66**, 2297 (1991).
- [74] M. Abe, P. Adamson, M. Borcean, D. Bortoletto, K. Bridges, S. P. Carman, S. Chattopadhyay, J. Coleman, N. M. Curfman, K. DeRose, T. Deshpande, S. Dimopoulos, C. J. Foot, J. C. Frisch, B. E. Garber, S. Geer, V. Gibson, J. Glick, P. W. Graham, S. R. Hahn, R. Harnik, L. Hawkins, S. Hindley, J. M. Hogan, Y. Jiang, M. A. Kasevich, R. J. Kellett, M. Kiburg, T. Kovachy, J. D. Lykken, J. March-Russell, J. Mitchell, M. Murphy, M. Nantel, L. E. Nobrega, R. K. Plunkett, S. Rajendran, J. Rudolph, N. Sachdeva, M. Safdari, J. K. Santucci, A. G. Schwartzman, I. Shipsey, H. Swan, L. R. Valerio, A. Vasonis, Y. Wang, and T. Wilkason, Matter-wave Atomic Gradiometer Interferometric Sensor (MAGIS-100), *Quantum Science and Technology* **6**, 044003 (2021).
- [75] L. Badurina, E. Bentine, D. Blas, K. Bongs, D. Bortoletto, T. Bowcock, K. Bridges, W. Bowden, O. Buchmueller, C. Burrage, J. Coleman, G. Elertas, J. Ellis, C. Foot, V. Gibson, M. Haehnelt, T. Harte, S. Hedges, R. Hobson, M. Holynski, T. Jones, M. Langlois, S. Lelouch, M. Lewicki, R. Maiolino, P. Majewski, S. Malik, J. March-Russell, C. McCabe, D. Newbold, B. Sauer, U. Schneider, I. Shipsey, Y. Singh, M. Uchida, T. Valenzuela, M. van der Grinten, V. Vaskonen, J. Vossebeeld, D. Weatherill, and I. Wilmut, AION: an atom interferometer observatory and network, *Journal of Cosmology and Astroparticle Physics* **2020** (05), 011.
- [76] J. Hartwig, S. Abend, C. Schubert, D. Schlippert, H. Ahlers, K. Posso-Trujillo, N. Gaaloul, W. Ertmer, and E. M. Rasel, Testing the universality of free fall with rubidium and ytterbium in a very large baseline atom interferometer, *New Journal of Physics* **17**, 035011 (2015).
- [77] L. Zhou *et al.*, Development of an atom gravimeter and status of the 10-meter atom interferometer for precision gravity measurement, *Gen. Rel. Gravit.* **43**, 1931 (2011).
- [78] S. Kulas, C. Vogt, A. Resch, J. Hartwig, S. Ganske, J. Matthias, D. Schlippert, T. Wendrich, W. Ertmer, E. M. Rasel, M. Damjanic, P. Weßels, A. Kohfeldt, E. Luvсандamdin, M. Schiemangk, C. Grzeschik, M. Krutzik, A. Wicht, A. Peters, S. Herrmann, and C. Lämmerzahl, Miniaturized lab system for future cold atom experiments in microgravity, *Microgravity Science and Technology* **29**, 37 (2016).
- [79] C. Vogt, M. Woltmann, S. Herrmann, C. Lämmerzahl, H. Albers, D. Schlippert, and E. M. R. and, Evaporative cooling from an optical dipole trap in microgravity, *Physical Review A* **101**, 013634 (2020).
- [80] D. Schlippert, C. Meiners, R. Rengelink, C. Schubert, D. Tell, É. Wodey, K. Zipfel, W. Ertmer, and E. Rasel, Matter-wave interferometry for inertial sensing and tests of fundamental physics, in *CPT and Lorentz Symmetry* (WORLD SCIENTIFIC, 2020).
- [81] M. Schilling, É. Wodey, L. Timmen, D. Tell, K. H. Zipfel, D. Schlippert, C. Schubert, E. M. Rasel, and J. Müller, Gravity field modelling for the hannover 10 m atom interferometer, *Journal of Geodesy* **94**, 10.1007/s00190-020-01451-y (2020).
- [82] M. Zaiser, J. Hartwig, D. Schlippert, U. Velte, N. Winter, V. Lebedev, W. Ertmer, and E. M. Rasel, Simple method for generating bose-einstein condensates in a weak hybrid trap, *Phys. Rev. A* **83**, 035601 (2011).
- [83] D. Guéry-Odelin, Mean-field effects in a trapped gas, *Physical Review A* **66**, 10.1103/physrev.66.033613 (2002).
- [84] P. Pedri, D. Guéry-Odelin, and S. Stringari, Dynamics of a classical gas including dissipative and mean-field effects, *Physical Review A* **68**, 10.1103/physrev.68.043608 (2003).
- [85] Y. Castin and R. Dum, Bose-einstein condensates in time dependent traps, *Physical Review Letters* **77**, 5315 (1996).

## ACKNOWLEDGEMENTS

This work is funded by the German Space Agency (DLR) with funds provided by the Federal Ministry of Economic Affairs and Energy (BMWi) due to an enactment of the German Bundestag under Grant Nos. DLR 50WM1641 (PRIMUS-III), DLR 50WM2041 (PRIMUS-IV), DLR 50WM1861 (CAL), DLR 50WM2060 (CARI-OQA), and DLR 50RK1957 (QGYRO). We acknowledge financial support from the Deutsche Forschungsgemeinschaft (DFG, German Research Foundation)—Project-ID 274200144—SFB 1227 DQ-mat within the projects A05, B07, and B09, and —Project-ID 434617780—SFB 1464 TerraQ within the projects A02 and A03 and Germany’s Excellence Strategy—EXC-2123 QuantumFrontiers—Project-ID 390837967 and from “Niedersächsisches Vorab” through the “Quantum- and Nano-Metrology (QUANOMET)” initiative within the Project QT3. A.H. and D.S. acknowledge support by the Federal Ministry of Education and Research (BMBF) through the funding program Photonics Research Germany under contract number 13N14875.

## AUTHOR CONTRIBUTIONS

W.E., E.M.R., and D.S. designed the experimental setup and the dipole trapping laser system. H.A., A.H., A.R., and D.S. contributed to the design, operation, and maintenance of the laser system and the overall setup. R.C., E.C. and N.G. set the theoretical framework of this work. H.A., R.C., C.S., and D.S. drafted the initial

manuscript. H.A., and R.C. performed the analysis of the data presented in this manuscript. H.A., and R.C. under lead of N.G. and C.S. performed the instability study. All authors discussed and evaluated the results and contributed to, reviewed, and approved of the manuscript.

#### **COMPETING INTERESTS**

All authors declare no competing interests.